Vehicle Velocity Estimation using Nonlinear Observers

Lars Imsland[a], Tor A. Johansen[a,c], Thor I. Fossen[a,c], Håvard Fjær Grip[a,c],

Jens C. Kalkkuhl[b], Avshalom Suissa[b]

[a]*SINTEF ICT, Applied Cybernetics, N-7465 Trondheim, Norway*
[b]*DaimlerChrysler Research and Technology, 70456 Stuttgart, Germany*
[c]*NTNU, Department of Engineering Cybernetics, N-7491 Trondheim, Norway*

Abstract

Nonlinear observers for estimation of lateral and longitudinal velocity of automotive vehicles are proposed. The observers are based on a sensor suite that is standard in many new cars, consisting of acceleration and yaw rate measurements in addition to wheel speed and steering angle measurements. Two approaches are considered: first, a modular approach where the estimated longitudinal velocity is used as input to the observer for lateral velocity, and second, a combined approach where all states are estimated in the same observer. Both approaches use a tire-road friction model, which is assumed to be known. It is also assumed that the road is flat. Stability of the observers is proven in the form of input-to-state stability of the observer error dynamics, under a structural assumption on the friction model. The assumption on the friction model is discussed in detail, and the observers are validated on experimental data from cars.

1. Introduction

Feedback control systems for active safety in automotive applications have entered production cars. Many of these systems (for instance yaw stabilization systems such as ESP (van Zanten, 2000)) have in common that the control action depends on information about vehicle velocity. However, the velocity is rarely measured directly and must therefore be inferred from other measurements, such as wheel speed, yaw rate, and acceleration measurements.

The main goal of this work is to develop computationally efficient nonlinear observers for vehicle velocity with theoretical stability guarantees. We propose two nonlinear observer structures: first, a modular cascaded observer structure where the estimation of lateral and longitudinal velocity is separated, and second, a combined observer for both velocities. We establish input-to-state stability (ISS) of both observer structures under a realistic condition on the friction model.

Nonlinear observers are used in order to take nonlinear dynamics (due mainly to highly nonlinear friction and Coriolis forces) into account and to obtain simple designs with few tuning knobs (as opposed to extended kalman filter (EKF) designs). Another significant advantage of the proposed approach over the EKF is that real-time solution of the Riccati differential equations is avoided, such that the observer can be implemented more efficiently in a low-cost electronic control unit.

A nonlinear tire-road friction model is used in order to fully exploit the lateral acceleration measurement. An important parameter in many friction models is the maximum tire-road friction coefficient μ_H, which is known to vary significantly with road conditions. We will assume that this parameter is known, that is, measured or estimated. While simultaneous estimation of velocity and μ_H might be a feasible path, we claim that estimation of μ_H requires special attention depending on the application of the observer, since it will be only weakly observable for some driving maneuvers, requiring monitoring,

resetting and other logic functions to be implemented (see e.g. Kalkkuhl, Johansen, & Ludemann, 2003). Estimation of friction parameters is therefore not considered in this paper. We also assume that the road bank and inclination angles are zero (or known), since these will introduce a gravity component in the horizontal acceleration measurements.

Earlier work on observers for estimation of lateral velocity is mainly based on linear or quasi-linear techniques, for example Fukada (1999), Venhovens and Naab (1999), Ungoren, Peng, and Tseng (2004), Farrelly and Wellstead (1996). A nonlinear observer linearizing the observer error dynamics is proposed in Kiencke and Daiss (1997), Kiencke and Nielsen (2000). The same type of observer, in addition to an observer based on forcing the dynamics of the nonlinear estimation error to the dynamics of a linear reference system, are investigated in Hiemer, vonVietinghoff, Kiencke, and Matsunaga (2005). The problem formulation there assumes that the longitudinal wheel forces are known, similarly to the observer implemented in ESP (van Zanten, 2000). In our work, we do not make this assumption, as such information is not always available.

An EKF is used for estimating vehicle velocity and tire forces in Ray (1995, 1997), thus without the explicit use of friction models. A similar, but simpler, approach is suggested in Farrelly and Wellstead (1996). An EKF based on a tire-road friction model which also includes estimation of the adhesion coefficient and road inclination angle is suggested in Suissa, Zomotor, and Böttiger (1996). In Best, Gordon, and Dixon (2000), the use of an EKF based on a nonlinear tire-road friction model is considered, which also includes estimation of cornering stiffness. The strategy proposed in Lu and Brown (2003) combines dynamic and kinematic models of the vehicle with numerical band-limited integration of the equations to provide a side-slip estimate. In Hac and Simpson (2000) the side-slip angle is estimated along with yaw rate in an approach which is similar to the one considered herein, but without yaw rate measurements. The approach is validated using experimental data, but no stability proofs are presented.

A unique feature of the work presented here is that explicit stability conditions are analyzed in a nonlinear setting, without resorting to linearizations.

2. Vehicle modeling

2.1. Rigid body dynamics

The geometry of the vehicle is illustrated in Fig. 1. The vehicle velocity is defined in a body-fixed coordinate system with the origin at the center of gravity (CG), the location of which is assumed constant. The x-axis points forward and the y-axis points to the left. There are also wheel-fixed coordinate systems aligned with each wheel and with origins at the wheel centers. The distance from the CG to each wheel center is denoted h_i, with i representing the wheel index. Together with the angles γ_i, this defines the vehicle geometry. Ignoring suspension dynamics, we assume that we can consider the vehicle a rigid body, for which the rigid body dynamics with respect to the CG
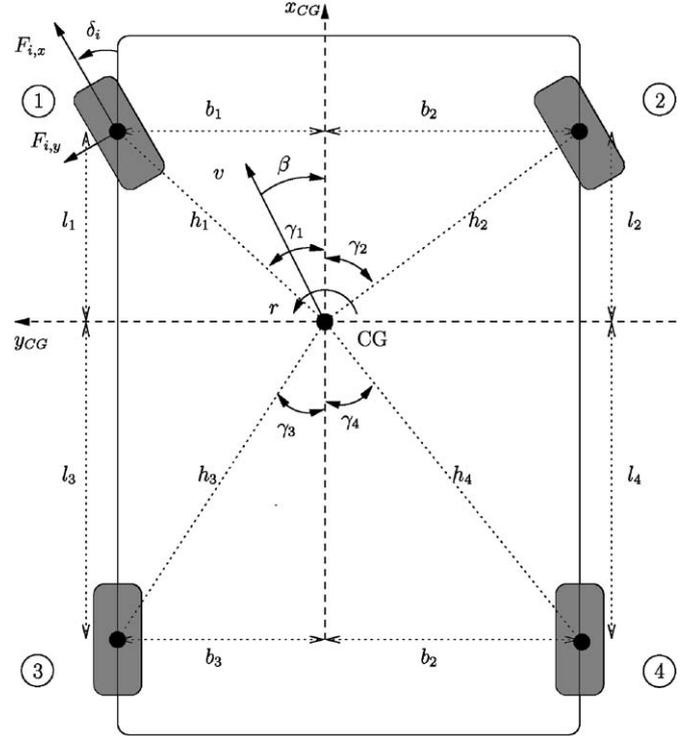

Fig. 1. Top view of vehicle: horizontal axis systems, geometric definitions, wheel forces, speed, slip angle and yaw rate.

coordinate system can be written (Kiencke & Nielsen, 2000)

$$\mathbf{M}\dot{v} + \mathbf{C}(v)v = \tau, \tag{1}$$

where v is a vector containing the body generalized velocities. The matrices $\mathbf{M}$ and $\mathbf{C}$ are the inertia, and the Coriolis and centripetal matrices, respectively. The vector τ consists of forces and torques acting on the vehicle; mainly friction forces acting via the wheels, but also gravitational and aerodynamic (wind and air resistance) forces.

By making the following assumptions:

- including only motion in the plane (ignore dynamics related to vertical motion, including roll and pitch),
- ignoring effect of caster and camber,
- including only forces caused by tire-road friction,

the vehicle dynamics are described by the longitudinal velocity v_x, lateral velocity v_y, and yaw rate r, for which

$$\mathbf{M} = \begin{pmatrix} m & 0 & 0 \\ 0 & m & 0 \\ 0 & 0 & J_z \end{pmatrix}, \quad \mathbf{C}(v) = \begin{pmatrix} 0 & -mr & 0 \\ mr & 0 & 0 \\ 0 & 0 & 0 \end{pmatrix}.$$

The generalized forces $\tau = (f_x, f_y, \tau_z)^\mathsf{T}$ are forces and torque acting on the vehicle generated by friction between the tires and the road. The friction forces $\mathbf{F}_i$ acting at each wheel (see Fig. 1) are functions of the velocity difference between the vehicle and the tires (cf. next section). These are transformed from the wheel coordinate systems to the body fixed coordinate system: in the body-fixed coordinate system, the forces generated by

tire-road friction for wheel i are $\mathbf{f}_i = (f_{i,x}, f_{i,y})^\mathsf{T} = \mathbf{R}(\delta_i)\mathbf{F}_i$, where $\mathbf{F}_i = (F_{i,x}, F_{i,y})$ are the forces acting on the wheel in the wheel-fixed coordinate system. The rotational matrices induced by the steering angles δ_i are

$$\mathbf{R}(\delta_i) = \begin{pmatrix} \cos \delta_i & -\sin \delta_i \\ \sin \delta_i & \cos \delta_i \end{pmatrix}.$$

For the torques, it is convenient to define the geometry vectors $\mathbf{g}_i := (-h_i \sin \psi_i, h_i \cos \psi_i)^\mathsf{T}$ where the angles ψ_i are defined as $\psi_1 = -\gamma_1$, $\psi_2 = \gamma_2$, $\psi_3 = \pi + \gamma_3$ and $\psi_4 = \pi - \gamma_4$. For wheel i, the generated torque about the vertical axis through the CG is then $\tau_{i,z} = \mathbf{g}_i^\mathsf{T} \mathbf{f}_i$. Summing forces and torques over all four wheels results in

$$\boldsymbol{\tau} = \sum_{i=1}^4 \begin{pmatrix} \mathbf{I}_{2 \times 2} \\ \mathbf{g}_i^\mathsf{T} \end{pmatrix} \mathbf{R}(\delta_i)\mathbf{F}_i. \tag{2}$$

2.2. Friction models

In most friction models, the friction forces are functions of tire slips, $\mathbf{F}_i = \mathbf{F}_i(\lambda_{i,x}, \lambda_{i,y})$, where the slips $\lambda_{i,x}$ and $\lambda_{i,y}$ are measures of the relative difference in vehicle and tire longitudinal and lateral velocity for wheel i. The definitions of tire slip we will use herein are

$$\lambda_{i,x} = \frac{\omega_i R_{\text{dyn}} - V_{i,x}}{V_{i,x}}, \quad \lambda_{i,y} = \sin \alpha_i,$$

where ω_i are wheel speeds (angular velocities) and R_{dyn} is the dynamic wheel radius, the tire slip angles are calculated as

$$\alpha_i = \delta_i - \arctan \frac{v_{i,y}}{v_{i,x}},$$

and $V_{i,x}$ are the velocities in x-direction of the wheel coordinate systems,

$$V_{i,x} = \sqrt{v_{i,x}^2 + v_{i,y}^2} \cos \alpha_i.$$

The longitudinal and lateral velocities of the wheel center in the body-fixed coordinate system are $v_{i,x} = v_x \pm r b_i$ and $v_{i,y} = v_y \pm r l_i$. For the tire slip angles to be well-defined, we assume that there is no reverse motion.

Assumption 1. We have $v_{i,x} > 0$ and $|\alpha_i| < \pi/2$, $i = 1, \ldots, 4$.

The tire slips depend on the vehicle states and the time-varying, measured steering angles $\boldsymbol{\delta} = (\delta_1, \ldots, \delta_4)^\mathsf{T}$ and wheel speeds $\boldsymbol{\omega} = (\omega_1, \ldots, \omega_4)^\mathsf{T}$. We will therefore use the notations $\mathbf{F}_i = \mathbf{F}_i(\lambda_{i,x}, \lambda_{i,y}) = \mathbf{F}_i(v_x, v_y, r, \delta_i, \omega_i)$ interchangeably, depending on the context.

We make the following assumption on the friction model:

Assumption 2. There exist a positive constant c_1, sets Δ, Ω and a convex set $X(\boldsymbol{\delta}, \boldsymbol{\omega})$, such that for all $\boldsymbol{\delta} \in \Delta$, $\boldsymbol{\omega} \in \Omega$ and $\boldsymbol{\chi} = (v_x, v_y, r)^\mathsf{T} \in X(\boldsymbol{\delta}, \boldsymbol{\omega})$, the friction model is continuously differentiable with respect to $\boldsymbol{\chi}$, $\|\partial \mathbf{F}_i(\boldsymbol{\chi}, \delta_i, \omega_i)/\partial \boldsymbol{\chi}\|$ are

bounded and

$$\sum_{i=1}^4 \left(\frac{\partial F_{i,y}(\boldsymbol{\chi}, \delta_i, \omega_i)}{\partial v_y} \cos \delta_i + \frac{\partial F_{i,x}(\boldsymbol{\chi}, \delta_i, \omega_i)}{\partial v_y} \sin \delta_i \right) < -c_1. \tag{3}$$

The physical meaning of this assumption is discussed in Appendix A. Note that (3) can be written $\partial f_y / \partial v_y \leqslant -c_1$.

Remark 1. The specification of the sets $X(\boldsymbol{\delta}, \boldsymbol{\omega})$ and Δ depends on the friction model used. For example, using linear friction models (see Section A.1), X depends on $\boldsymbol{\delta}$ only:

$$\Delta = \{\delta_i : |\delta_i| \leqslant \bar{\delta}, \ i = 1, \ldots, 4\},$$

$$X(\boldsymbol{\delta}) = \{\boldsymbol{\chi} = (v_x, v_y, r)^\mathsf{T} : |\alpha_i| \leqslant \bar{\alpha}, \ |r| \leqslant \bar{r}, \ v_x > \bar{r}b_i\},$$

where $\bar{\delta}$, $\bar{\alpha}$ and $\bar{r}$ are positive constants. Note that α_i depends on δ_i.

The following result regarding the friction forces holds due to Assumption 2:

Lemma 1. *There exist positive constants c_i, $i = 1, \ldots, 6$ such that for all $\boldsymbol{\chi}, \hat{\boldsymbol{\chi}} \in X(\boldsymbol{\delta}, \boldsymbol{\omega})$, $\boldsymbol{\delta} \in \Delta$, $\boldsymbol{\omega} \in \Omega$,*

$$\tilde{v}_y \sum_{i=1}^4 (0 \ 1) \mathbf{R}(\delta_i)(\mathbf{F}_i(\boldsymbol{\chi}, \delta_i, \omega_i) - \mathbf{F}_i(\hat{\boldsymbol{\chi}}, \delta_i, \omega_i))$$
$$\leqslant -c_1 \tilde{v}_y^2 + c_2 |\tilde{r}||\tilde{v}_y| + c_3 |\tilde{v}_x||\tilde{v}_y|, \tag{4a}$$

$$\frac{1}{J_z} \sum_{i=1}^4 \mathbf{g}_i^\mathsf{T} \mathbf{R}(\delta_i)(\mathbf{F}_i(\boldsymbol{\chi}, \delta_i, \omega_i) - \mathbf{F}_i(\hat{\boldsymbol{\chi}}, \delta_i, \omega_i))$$
$$\leqslant c_4 |\tilde{v}_y| + c_5 |\tilde{r}| + c_6 |\tilde{v}_x|, \tag{4b}$$

where $(\tilde{v}_x, \tilde{v}_y, \tilde{r}) := \boldsymbol{\chi} - \hat{\boldsymbol{\chi}}$.

Proof. Define $h(\boldsymbol{\chi}, \boldsymbol{\delta}, \boldsymbol{\omega}) := \sum_{i=1}^4 (0 \ 1) \mathbf{R}(\delta_i) \mathbf{F}_i(\boldsymbol{\chi}, \delta_i, \omega_i)$. The *mean value theorem* gives

$$h(\boldsymbol{\chi}, \boldsymbol{\delta}, \boldsymbol{\omega}) - h(\hat{\boldsymbol{\chi}}, \boldsymbol{\delta}, \boldsymbol{\omega})$$
$$= \frac{\partial h(\boldsymbol{\chi}', \boldsymbol{\delta}, \boldsymbol{\omega})}{\partial v_y} \tilde{v}_y + \frac{\partial h(\boldsymbol{\chi}', \boldsymbol{\delta}, \boldsymbol{\omega})}{\partial r} \tilde{r} + \frac{\partial h(\boldsymbol{\chi}', \boldsymbol{\delta}, \boldsymbol{\omega})}{\partial v_x} \tilde{v}_x,$$

where $\boldsymbol{\chi}'$ is some point on the line segment between $\boldsymbol{\chi}$ and $\hat{\boldsymbol{\chi}}$. Multiplying this expression with $\tilde{v}_y$, we get

$$\tilde{v}_y \sum_{i=1}^4 (0 \ 1) \mathbf{R}(\delta_i)(\mathbf{F}_i(\boldsymbol{\chi}, \delta_i, \omega_i) - \mathbf{F}_i(\hat{\boldsymbol{\chi}}, \delta_i, \omega_i))$$

$$= \sum_{i=1}^4 \left(\cos \delta_i \frac{\partial F_{i,y}(z_i)}{\partial v_y} + \sin \delta_i \frac{\partial F_{i,x}(z_i)}{\partial v_y} \right) \tilde{v}_y^2$$

$$+ \sum_{i=1}^4 \left(\cos \delta_i \frac{\partial F_{i,y}(z_i)}{\partial r} + \sin \delta_i \frac{\partial F_{i,x}(z_i)}{\partial r} \right) \tilde{r} \tilde{v}_y$$

$$+ \sum_{i=1}^4 \left(\cos \delta_i \frac{\partial F_{i,y}(z_i)}{\partial v_x} + \sin \delta_i \frac{\partial F_{i,x}(z_i)}{\partial v_x} \right) \tilde{v}_x \tilde{v}_y,$$

where $z_i = (\boldsymbol{\chi}', \delta_i, \omega_i)$. From Assumption 2, we arrive at (4a). According to Khalil (2002, Lemma 3.1), the Lipschitz-type condition (4b) holds on $X(\boldsymbol{\delta}, \boldsymbol{\omega})$ since $\mathbf{F}$ has continuous and upper bounded partial derivatives. $\square$

2.3. Measurements

The measurements used are summarized below

Symbol	Measurement
a_x, a_y	Longitudinal and lateral acceleration
r	Yaw rate
ω_i	Wheel speed (angular velocity) for wheel i
δ_i	Steering angle for wheel i

All these measurements, with the possible exception of a_x, can be considered standard in modern cars with yaw stabilization (anti-skid) systems, such as the Bosch ESP system (van Zanten, 2000). The acceleration and yaw rate sensors are assumed located in the CG (or corrected if this is not the case), and to have bias and slow drift components removed. The acceleration measurements are corrected for gravity components due to vehicle roll/pitch, based on suspension stiffness and the assumption of a flat road.

2.4. System model

The system model used in this paper is (1) with the measured accelerations replacing friction forces in the velocity derivatives:

$$\dot{v}_x = v_y r + a_x, \tag{5a}$$

$$\dot{v}_y = -v_x r + a_y, \tag{5b}$$

$$\dot{r} = \frac{1}{J_z} \sum_{i=1}^{4} \mathbf{g}_i^\mathsf{T} \mathbf{R}(\delta_i) \mathbf{F}_i(\mathbf{x}, \delta_i, \omega_i). \tag{5c}$$

This allows using the friction model as a measurement equation based on (2). This model is often denoted the two-track model.

In observer design, one often requires that the states to be observed must exist for all future time. While in the present case this may be obvious from physics, we include a result on forward completeness for (5).

Assumption 3. The accelerations and friction forces are bounded, i.e. $|a_x| \leqslant \bar{a}_x$, $|a_y| \leqslant \bar{a}_y$, and $|\mathbf{F}_i| \leqslant \bar{\mathbf{F}}$.

Lemma 2 (*Forward completeness*). *For all initial conditions, the solutions of system* (5) *exist for all future time.*

Proof (*Outline*). Let $\mathbf{x} = (v_x, v_y, r)^\mathsf{T}$, define $V(\mathbf{x}) = \frac{1}{2}\mathbf{x}^\mathsf{T}\mathbf{x} + k$. Using Assumption 3, it is easy to show that k can be chosen such that $\dot{V} \leqslant V$, implying forward completeness (Angeli & Sontag, 1999). $\square$

3. Modular observer design

The modular observer structure is illustrated in Fig. 2. The longitudinal velocity observer uses mainly information of wheel speed, but also yaw rate and longitudinal acceleration. The longitudinal velocity estimate is used together with measurements of lateral acceleration, yaw rate, wheel speeds, and steering angles to estimate lateral velocity. The model described in Section 2 will be simplified for each of the observer modules: when estimating longitudinal velocity, we ignore the lateral (v_y and r) dynamics, and when estimating lateral velocity, we assume that v_x is known, thus using only two dynamic states. The main motivation for structuring the observer in this way is that it results in a modular design with few tuning knobs. Also, since we will prove stability properties independently for the modules (before proving overall stability by exploiting the cascaded structure), they can be tuned independently, and one can also imagine replacing the module for longitudinal velocity, if a better estimate is available (for instance from an observer with access to more information such as engine and brake measurements).

3.1. Estimation of longitudinal velocity

When estimating longitudinal velocity, we use a model including v_x only, omitting the Coriolis term in (5a):

$$\dot{v}_x = a_x. \tag{6}$$

The wheel speed measurements ω_i are transformed to measurements of v_x, assuming zero slips. Using $v_{i,x} = R_{\mathrm{dyn}}\omega_i \cos\delta_i$ and $v_{i,x} = v_x \pm b_i r$, we get the following expression for the transformed measurement from wheel i:

$$v_{x,i} = R_{\mathrm{dyn}}\omega_i \cos\delta_i \pm b_i r. \tag{7}$$

Using these, we propose the following observer:

$$\dot{\hat{v}}_x = a_x + \sum_{i=1}^{4} K_i(a_x, \boldsymbol{\omega})(v_{x,i} - \hat{v}_x). \tag{8}$$

The observer gains K_i depend on the longitudinal acceleration and the wheel speed measurements (and possibly other information), to reflect when ω_i are expected to provide good estimates of v_x, that is, when the tire slips are low. For the sake of brevity we do not elaborate on this, but refer to similar work in Kiencke and Nielsen (2000), Imsland, Johansen,
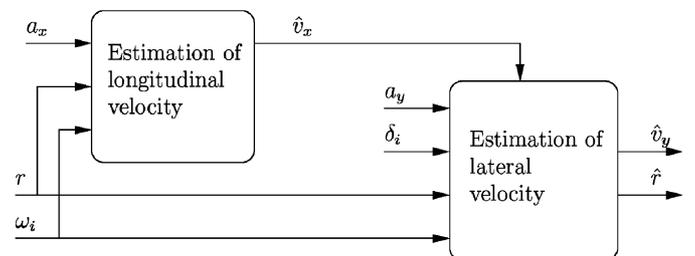

Fig. 2. Modular observer structure.

Fossen, Kalkkuhl, and Suissa (2005). For the stability results to follow, we make the following assumption about the gains:

Assumption 4. The gains $K_i(a_x, \omega)$ are piecewise continuous in time and bounded, $K_i(a_x, \omega) > k_x > 0$.

Assuming $v_{x,i} = v_x$ (which requires that the lateral and longitudinal slips are zero), it is trivial to show that the observer error dynamics are uniformly globally exponentially stable, since the gains are positive. However, in general, we have non-zero slips and $v_{x,i} \neq v_x$. If the slips were known, the correct equation (for each wheel) would be[1]

$$v_x = \frac{1}{1 + \lambda_{i,x}} \frac{\cos(\delta_i - \alpha_i)}{\cos \alpha_i} R_{\text{dyn}} \omega_i \pm b_i r.$$

Define $\tilde{v}_x := v_x - \hat{v}_x$. Then $\sum_{i=1}^{4} K_i(a_x, \omega)(v_{x,i} - \hat{v}_x) = \sum_{i=1}^{4} K_i(a_x, \omega)\tilde{v}_x + u$, where

$$u = \sum_{i=1}^{4} K_i(a_x, \omega) \left(\cos \delta_i - \frac{\cos(\delta_i - \alpha_i)}{(1 + \lambda_{i,x}) \cos \alpha_i} \right) R_{\text{dyn}} \omega_i \quad (9)$$

is an error-term due to non-zero slip. Consequently, the error dynamics from (6) and (8) are

$$\dot{\tilde{v}}_x = - \sum_{i=1}^{4} K_i(a_x, \omega)\tilde{v}_x + u. \quad (10)$$

As noted above, $\tilde{v}_x = 0$ is globally exponentially stable if $u = 0$. During acceleration, including turning and braking, $u \neq 0$, and this affects the observer error. Observer properties that are natural to aim for are that the influence of u should not lead to divergence of $\tilde{v}_x$, that when u is small, the influence on $\tilde{v}_x$ should be small, and that when u vanishes, $\tilde{v}_x$ should go to zero. These properties correspond to ISS (Khalil, 2002; Sontag & Wang, 1995), characterized by convergence of the zero-input response and that the zero-state response is bounded for bounded inputs.

Theorem 1. *Assume that the wheel speeds ω_i are bounded. Then the observer error dynamics (10) are globally ISS with respect to $u(t)$, and*

$$|\tilde{v}_x(t)| \leqslant |\tilde{v}_x(t_0)| e^{-(k_x/2)(t-t_0)} + \frac{2}{k_x} \left(\sup_{t_o \leqslant \tau \leqslant t} |u(\tau)| \right). \quad (11)$$

Proof. Boundedness of the wheel speeds implies that $\sup_{t_o \leqslant \tau \leqslant t} |u(\tau)|$ exists. Then (11) follows from (10), implying global ISS (Khalil, 2002, Definition 4.7). $\quad \square$

Note that we have disregarded the Coriolis term in the observer model (6) and in the analysis. The effect of the Coriolis term could be included in $u(t)$.

3.2. Estimation of lateral velocity

When estimating the lateral velocity, we will first assume that v_x is known. This assumption is removed in Section 3.3 by analyzing both observers together. Thus, in this section we let $\mathbf{x} = (v_y, r)^\mathsf{T}$ and lump the time-varying parameters in $\boldsymbol{\theta} = (v_x, \boldsymbol{\delta}^\mathsf{T}, \boldsymbol{\omega}^\mathsf{T})^\mathsf{T}$. The model used is then[2]

$$\dot{v}_y = -v_x r + a_y, \quad (12a)$$

$$\dot{r} = \frac{1}{J_z} \sum_{i=1}^{4} \mathbf{g}_i^\mathsf{T} \mathbf{R}(\delta_i) \mathbf{F}_i. \quad (12b)$$

Based on this model, we propose the following observer:

$$\dot{\hat{v}}_y = -v_x r + a_y - K_{v_y} \left(m a_y - \sum_{i=1}^{4} (0\ 1) \mathbf{R}(\delta_i) \hat{\mathbf{F}}_i \right), \quad (13a)$$

$$\dot{\hat{r}} = \frac{1}{J_z} \sum_{i=1}^{4} \mathbf{g}_i^\mathsf{T} \mathbf{R}(\delta_i) \hat{\mathbf{F}}_i + K_r(r - \hat{r}). \quad (13b)$$

Define the error variables $\tilde{v}_y := v_y - \hat{v}_y$ and $\tilde{r} := r - \hat{r}$, and $\tilde{\mathbf{x}} := (\tilde{v}_y, \tilde{r})^\mathsf{T}$. We will make use of the following fact:

Fact 1. *By completing squares,*

$$-a\xi_1^2 + b|\xi_1||\xi_2| = \frac{b^2}{4a}\xi_2^2 - \left(\sqrt{a}|\xi_1| - \frac{b}{2\sqrt{a}}|\xi_2| \right)^2.$$

Define (with some abuse of notation) the sets $X(\boldsymbol{\theta}) := \{\mathbf{x} : (v_x, \mathbf{x}) \in X(\boldsymbol{\delta}, \boldsymbol{\omega})\}$ and[3] $X_s(\rho; \boldsymbol{\theta}) = \{\mathbf{x} : B_\rho(\mathbf{x}) \subset X(\boldsymbol{\theta})\} \subset X(\boldsymbol{\theta})$. The observer error dynamics are

$$\dot{\tilde{v}}_y = K_{v_y} \sum_{i=1}^{4} (0\ 1) \mathbf{R}(\delta_i)(\mathbf{F}_i - \hat{\mathbf{F}}_i), \quad (14a)$$

$$\dot{\tilde{r}} = \frac{1}{J_z} \sum_{i=1}^{4} \mathbf{g}_i^\mathsf{T} \mathbf{R}(\delta_i)(\mathbf{F}_i - \hat{\mathbf{F}}_i) - K_r \tilde{r}. \quad (14b)$$

Theorem 2. *Assume that ρ and Θ are such that $\forall \boldsymbol{\theta} \in \Theta$ and $\forall t \geqslant 0$, $\mathbf{x}(t) \in X_s(\rho; \boldsymbol{\theta})$. For some $k_r > 0$, let the observer gains be chosen such that*

$$K_{v_y} > 0, \quad (15)$$

$$K_r > k_r + c_5 + \frac{(K_{v_y}c_2 + c_4)^2}{2K_{v_y}c_1}. \quad (16)$$

Then, if $\|\tilde{\mathbf{x}}(0)\| \leqslant \rho$, the state $\hat{\mathbf{x}}(t)$ of the observer (13) converges to the state $\mathbf{x}(t)$ of the system (12), and the origin of the observer error dynamics (14) is uniformly exponentially stable.

---

[1] If slip estimates are available from other information than the velocity estimates, they could be included in the equation for $v_{x,i}$.

[2] For brevity, we write $\mathbf{F}_i$ to denote $\mathbf{F}_i(v_x, v_y, r, \delta_i, \omega_i)$ and $\hat{\mathbf{F}}_i$ to denote $\mathbf{F}_i(v_x, \hat{v}_y, \hat{r}, \delta_i, \omega_i)$ in this section.
[3] $B_\rho(\mathbf{x}) := \{\mathbf{z} : \|\mathbf{z} - \mathbf{x}\| \leqslant \rho\}$ is the closed ball of radius ρ, centered at $\mathbf{x}$.

Proof. Define the Lyapunov function candidate $V(\tilde{\mathbf{x}}) := \frac{1}{2}(\tilde{v}_y^2 + \tilde{r}^2)$. The time derivative along the trajectories of (14) is

$$
\dot{V} = \tilde{v}_y\left(K_{v_y}\sum_{i=1}^{4}(0\ 1)\mathbf{R}(\delta_i)(\mathbf{F}_i - \hat{\mathbf{F}}_i)\right)
$$

$$
+ \tilde{r}\left(\frac{1}{J_z}\sum_{i=1}^{4}\mathbf{g}_i^\mathsf{T}\mathbf{R}(\delta_i)(\mathbf{F}_i - \hat{\mathbf{F}}_i) - K_r\tilde{r}\right).
$$

Letting $\hat{v}_x = v_x$ in Lemma 1, the following holds if $\hat{x} \in X(\theta)$:

$$
\tilde{v}_y\sum_{i=1}^{4}(0\ 1)\mathbf{R}(\delta_i)(\mathbf{F}_i - \hat{\mathbf{F}}_i) \leqslant -c_1\tilde{v}_y^2 + c_2|\tilde{r}||\tilde{v}_y|,
$$

$$
\frac{1}{J_z}\sum_{i=1}^{4}\mathbf{g}_i^\mathsf{T}\mathbf{R}(\delta_i)(\mathbf{F}_i - \hat{\mathbf{F}}_i) \leqslant c_4|\tilde{v}_y| + c_5|\tilde{r}|.
$$

Using this, $\dot{V}$ can be upper bounded:

$$
\dot{V} \leqslant -K_{v_y}c_1\tilde{v}_y^2 + K_{v_y}c_2|\tilde{r}||\tilde{v}_y| + c_4\tilde{r}|\tilde{v}_y| + c_5\tilde{r}|\tilde{r}| - K_r\tilde{r}^2,
$$

$$
\leqslant (K_{v_y}c_2 + c_4)|\tilde{r}||\tilde{v}_y| - K_{v_y}c_1\tilde{v}_y^2 + c_5\tilde{r}|\tilde{r}| - K_r\tilde{r}^2.
$$

By Fact 1 and (15),

$$
\dot{V} \leqslant \frac{(K_{v_y}c_2 + c_4)^2}{2K_{v_y}c_1}\tilde{r}^2 - \frac{K_{v_y}c_1}{2}\tilde{v}_y^2 + c_5\tilde{r}|\tilde{r}| - K_r\tilde{r}^2
$$

$$
- \left(\sqrt{\frac{K_{v_y}c_1}{2}}|\tilde{v}_y| - \frac{(K_{v_y}c_2 + c_4)}{\sqrt{2K_{v_y}c_1}}|\tilde{r}|\right)^2.
$$

We see that, due to (16),

$$
\dot{V} \leqslant -\frac{K_{v_y}c_1}{2}\tilde{v}_y^2 - k_r\tilde{r}^2 \tag{17}
$$

is uniformly negative definite for $\mathbf{x}, \hat{\mathbf{x}} \in X(\theta)$.

By assumption, $\forall t > 0$, $\mathbf{x}(t) \in X_s(\rho, \theta(t)) \subset X(\theta(t))$, and we must show that $\forall t > 0$, $\hat{\mathbf{x}}(t) \in X(\theta(t))$. Since $\mathbf{x}(t) \in X_s(\rho; \theta(t))$ and $\|\tilde{\mathbf{x}}(0)\| \leqslant \rho$, $\hat{\mathbf{x}}(0) \in X(\theta(0))$. From the above, $\mathrm{d}/\mathrm{d}t\|\tilde{\mathbf{x}}\| = \dot{V}/\|\tilde{\mathbf{x}}\| < 0$, which means that $\forall t > 0$, $\|\tilde{\mathbf{x}}(t)\| \leqslant \rho$, and hence $\hat{\mathbf{x}}(t)$ will remain in $X(\theta(t))$. Thus, from (17) and standard Lyapunov theory (Khalil, 2002), we conclude the theorem. $\square$

Remark 2. The observer for v_y (13a) could use the estimate $\hat{r}$ instead of the measured r in the Coriolis term (replacing $v_x r$ with $v_x\hat{r}$). The bound (16) would then depend on an upper bound on v_x (Imsland et al., 2005).

3.3. Cascaded stability

In the previous section, it was assumed that the longitudinal velocity v_x was known. In this section, we analyze stability properties when using the estimate $\hat{v}_x$ instead of v_x.
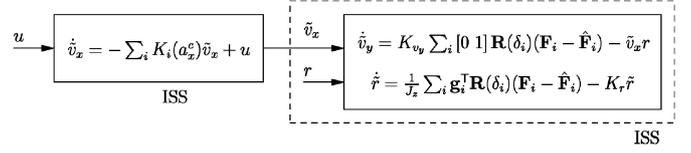

Fig. 3. Stability properties of the modular observer error dynamics.

Since $\hat{v}_x = v_x - \tilde{v}_x$, (14a) in the lateral velocity observer error dynamics must be replaced with[4]

$$
\dot{\tilde{v}}_y = K_{v_y}\sum_{i=1}^{4}(0\ 1)\mathbf{R}(\delta_i)(\mathbf{F}_i - \hat{\mathbf{F}}_i) - \tilde{v}_x r.
$$

Using the Lyapunov function from the proof of Theorem 2 and letting $k_y = \min(K_{v_y}c_1/2, k_r)$, it can be shown that

$$
\dot{V} \leqslant -\frac{K_{v_y}c_1}{2}\tilde{v}_y^2 - k_r\tilde{r}^2 + |\tilde{v}_y||r||\tilde{v}_x| + c_3|\tilde{v}_y||\tilde{v}_x| + c_6|\tilde{r}||\tilde{v}_x|
$$

$$
\leqslant -k_y\|\tilde{\mathbf{x}}\|^2 + \kappa\|\tilde{\mathbf{x}}\||\tilde{v}_x|,
$$

where $\kappa = \sqrt{2}\max(\bar{r} + c_3, c_6)$ and $\bar{r}$ is an upper bound on $r(t)$. It follows that

$$
\dot{V} \leqslant -\frac{k_y}{2}\|\tilde{\mathbf{x}}\|^2 \quad \forall\|\tilde{\mathbf{x}}\| \geqslant \frac{2\kappa}{k_y}|\tilde{v}_x|,
$$

implying ISS by Khalil (2002, Theorem 4.19), namely

$$
\|\tilde{\mathbf{x}}(t)\| \leqslant \|\tilde{\mathbf{x}}(t_0)\|\mathrm{e}^{-(k_y/2)(t-t_0)} + \frac{2\kappa}{k_y}\left(\sup_{t_o \leqslant \tau \leqslant t}|\tilde{v}_x(\tau)|\right) \tag{18}
$$

assuming the supremum exists, and also that $\tilde{\mathbf{x}}(t) \to 0$ if $\tilde{v}_x(t) \to 0$ as $t \to \infty$. Since the conditions of Theorem 2 do not hold globally, we state a local variant of ISS.

Corollary 1. *Assume that the conditions of Theorem 2 hold for all $(\delta, \omega) \in \Delta \times \Omega$ on $\|\tilde{\mathbf{x}}\| \leqslant d_x$ and $|u| \leqslant d_u$. Then there exist positive constants k_1 and k_2 such that (18) holds for $\|\tilde{\mathbf{x}}(t_0)\| < k_1$ and $\sup_{t>t_0}|u(t)| < k_2$.*

Proof. The result follows from the definition of local ISS (Khalil, 2002, p. 192) and the above. $\square$

The cascaded stability is illustrated in Fig. 3.

4. Combined observer design

In this section, we combine longitudinal and lateral velocity estimation in the same observer, and therefore let $\mathbf{x} = (v_x, v_y, r)^\mathsf{T}$. The main advantage of this is that the Coriolis term can be included in the equation for longitudinal velocity.

---

[4] $\hat{\mathbf{F}}_i$ is now used for $\mathbf{F}_i(\hat{v}_x, \hat{v}_y, \hat{r}, \delta_i, \omega_i)$.

The system model is given by (5), for which we propose the following observer[5] :

$$\dot{\hat{v}}_x = \hat{v}_y r + a_x + \sum_{i=1}^{4} K_i(a_x, \boldsymbol{\omega})(v_{x,i} - \hat{v}_x), \tag{19a}$$

$$\dot{\hat{v}}_y = -\hat{v}_x r + a_y - K_{v_y}\left(ma_y - \sum_{i=1}^{4}(0\ 1)\mathbf{R}(\delta_i)\hat{\mathbf{F}}_i\right), \tag{19b}$$

$$\dot{\hat{r}} = \frac{1}{J_z}\sum_{i=1}^{4}\mathbf{g}_i^\mathsf{T}\mathbf{R}(\delta_i)\hat{\mathbf{F}}_i + K_r(r - \hat{r}). \tag{19c}$$

As in Section 3.1, we write $\sum_{i=1}^{4}K_i(a_x, \boldsymbol{\omega})(v_{x,i} - \hat{v}_x) = \sum_{i=1}^{4}K_i(a_x, \boldsymbol{\omega})\tilde{v}_x + u$, and the goal of this section is to show that the observer error dynamics,

$$\dot{\tilde{v}}_x = \tilde{v}_y r - \sum_{i=1}^{4}K_i(a_x, \boldsymbol{\omega})\tilde{v}_x + u, \tag{20a}$$

$$\dot{\tilde{v}}_y = -\tilde{v}_x r + K_{v_y}\sum_{i=1}^{4}(0\ 1)\mathbf{R}(\delta_i)(\mathbf{F}_i - \hat{\mathbf{F}}_i), \tag{20b}$$

$$\dot{\tilde{r}} = \frac{1}{J_z}\sum_{i=1}^{4}\mathbf{g}_i^\mathsf{T}\mathbf{R}(\delta_i)(\mathbf{F}_i - \hat{\mathbf{F}}_i) - K_r\tilde{r}, \tag{20c}$$

is ISS with $u(t)$ as input.

We redefine $X_s(\rho; \boldsymbol{\delta}, \boldsymbol{\omega}) := \{\mathbf{x} : B_\rho(\mathbf{x}) \subset X(\boldsymbol{\delta}, \boldsymbol{\omega})\} \subset X(\boldsymbol{\delta}, \boldsymbol{\omega})$. We first show that with $u(t) = 0$, the origin of the observer error dynamics is exponentially stable:

Theorem 3. *Assume that ρ and Δ, Ω are such that $\forall(\boldsymbol{\delta}, \boldsymbol{\omega}) \in \Delta \times \Omega$, $\forall t \geqslant 0$, $\mathbf{x}(t) \in X_s(\rho; \boldsymbol{\delta}, \boldsymbol{\omega})$, and that $\forall t > 0$, $u(t) = 0$. Let the observer gains be chosen such that*

$$K_{v_y} > 0, \tag{21}$$

$$k_x > \frac{1}{4}\frac{K_{v_y}c_3^2}{c_1}, \tag{22}$$

$$K_r > c_5 + \frac{c_7}{4k_x K_{v_y}c_1 - (K_{v_y}c_3)^2}, \tag{23}$$

where $c_7 = (K_{v_y}c_2 + c_4)(k_x(K_{v_y}c_2 + c_4) - \frac{1}{2}K_{v_y}c_3c_6) + c_6(\frac{1}{2}K_{v_y}c_3(K_{v_y}c_2 + c_4) + K_{v_y}c_1c_6)$. Then, if $\|\tilde{\mathbf{x}}(0)\| \leqslant \rho$, the state $\hat{\mathbf{x}}(t)$ of the observer (19) converges to the state $\mathbf{x}(t)$ of the system (5), and the origin of the observer error dynamics (20) is uniformly exponentially stable.

Proof. Define the Lyapunov function candidate $V(\tilde{\mathbf{x}}) := \frac{1}{2}(\tilde{v}_x^2 + \tilde{v}_y^2 + \tilde{r}^2)$. The time derivative along the trajectories

---

[5] In this section, we use $\mathbf{F}_i$ to denote $\mathbf{F}_i(v_x, v_y, r, \delta_i, \omega_i)$ and $\hat{\mathbf{F}}_i$ to denote $\mathbf{F}_i(\hat{v}_x, \hat{v}_y, \hat{r}, \delta_i, \omega_i)$.

of (20) is

$$\dot{V} = \tilde{v}_x\left(\tilde{v}_y r - \sum_{i=1}^{4}K_i(a_x, \boldsymbol{\omega})\tilde{v}_x\right)$$

$$+ \tilde{v}_y\left(-\tilde{v}_x r + K_{v_y}\sum_{i=1}^{4}(0\ 1)\mathbf{R}(\delta_i)(\mathbf{F}_i - \hat{\mathbf{F}}_i)\right)$$

$$+ \tilde{r}\left(\frac{1}{J_z}\sum_{i=1}^{4}\mathbf{g}_i^\mathsf{T}\mathbf{R}(\delta_i)(\mathbf{F}_i - \hat{\mathbf{F}}_i) - K_r\tilde{r}\right).$$

Using Lemma 1, this can be upper bounded when $\hat{x} \in X(\delta, \omega)$:

$$\dot{V} \leqslant -k_x\tilde{v}_x^2 - K_{v_y}c_1\tilde{v}_y^2 + K_{v_y}c_2|\tilde{r}||\tilde{v}_y| + K_{v_y}c_3|\tilde{v}_x||\tilde{v}_y|$$

$$+ c_4\tilde{r}|\tilde{v}_y| + c_5\tilde{r}|\tilde{r}| + c_6\tilde{r}|\tilde{v}_x| - K_r\tilde{r}^2$$

$$= -|\tilde{\mathbf{x}}|^\mathsf{T}A|\tilde{\mathbf{x}}|,$$

where $|\tilde{\mathbf{x}}| = (|\tilde{v}_x|, |\tilde{v}_y|, |\tilde{r}|)^\mathsf{T}$ and the matrix A is defined as

$$A := \begin{pmatrix} k_x & -\frac{1}{2}K_{v_y}c_3 & -\frac{1}{2}c_6 \\ -\frac{1}{2}K_{v_y}c_3 & K_{v_y}c_1 & -\frac{1}{2}K_{v_y}c_2 - \frac{1}{2}c_4 \\ -\frac{1}{2}c_6 & -\frac{1}{2}K_{v_y}c_2 - \frac{1}{2}c_4 & K_r - c_5 \end{pmatrix}.$$

To show that $\dot{V}$ is negative definite, we show that the conditions (21)–(23) imply that all principal minors of A are positive, and therefore that A is positive definite.

The second principal minor, $k_x K_{v_y}c_1 - \frac{1}{4}(K_{v_y}c_3)^2$, is positive due to (21) and (22), which also ensures the positivity of the first principal minor (k_x). The third principal minor (the determinant), calculated based on the third column, is

$$(K_r - c_5)(k_x K_{v_y}c_1 - \frac{1}{4}(K_{v_y}c_3)^2)$$

$$+ \frac{1}{2}(K_{v_y}c_2 + c_4)\det A_{2,3} - \frac{1}{2}c_6\det A_{1,3},$$

where $A_{i,j}$ is the 2×2 matrix produced by removing row i and column j from A. Noting that $\det A_{2,3}$ and $\det A_{1,3}$ do not depend on K_r, we see that the determinant can be made positive by choosing K_r large enough. After some tedious calculations, we end up with the bound (23). The remainder of the proof, showing $\hat{x} \in X(\delta, \omega)$, follows as in the proof of Theorem 2. $\square$

Using the Lyapunov function from the above proof, a non-zero $u(t)$ gives (for small $\tilde{\mathbf{x}}$)

$$\dot{V} \leqslant -\lambda_{\min}(A)\|\tilde{\mathbf{x}}\|^2 + \|\tilde{\mathbf{x}}\||u|,$$

implying that

$$\|\tilde{\mathbf{x}}(t)\| \leqslant \|\tilde{\mathbf{x}}(t_0)\|e^{-(\lambda_{\min}(A)/2)(t-t_0)} + \frac{2}{\lambda_{\min}(A)}\left(\sup_{t_o \leqslant \tau \leqslant t}|u(\tau)|\right), \tag{24}$$

assuming the supremum exists. Since the conditions in Theorem 3 do not hold globally, we conclude as in Section 3.3 a local variant of ISS.

Corollary 2. *Assume that the conditions of Theorem 3 hold for all $(\boldsymbol{\delta}, \boldsymbol{\omega}) \in \varDelta \times \varOmega$ on $\|\tilde{\mathbf{x}}\| \leqslant d_x$ and $|u| \leqslant d_u$. Then there exist positive constants k_1 and k_2 such that (24) holds for $\|\tilde{\mathbf{x}}(t_0)\| < k_1$ and $\sup_{t>t_0} |u(t)| < k_2$.*

5. Observer robustness

The analysis up to this point has been based on the assumption of no model-plant mismatch; in particular that the friction model used in the observer represents the real relation between wheel slips and friction forces. Although the exponential stability results obtained imply some robustness (Khalil, 2002), in this section we will show that the observer error dynamics are also ISS with respect to errors in the friction model. Furthermore, assuming that Assumption 2 holds globally for the friction model used in the observer, we will show that the observer error (and thus the states of the observer) remains bounded for any initial conditions regardless of model-plant mismatches. We consider only the observer proposed in Section 4, noting that similar results can be shown in the same way for the lateral velocity observer in Section 3.2.

Assume that the observer friction model ($\mathbf{F}_i$) is related to the real relation between wheel slips and wheel forces, denoted $\mathbf{F}_{r,i}$, in the following way:

$$\mathbf{F}_i(\mathbf{x}, \delta_i, \omega_i) = \mathbf{F}_{r,i}(\mathbf{x}, \delta_i, \omega_i) + \Delta\mathbf{F}_i(\mathbf{x}, \delta_i, \omega_i),$$

where $\Delta\mathbf{F}$ represents the model-plant mismatch. The difference between the real forces and the observer forces can then be written

$$\mathbf{F}_{r,i}(\mathbf{x}, \delta_i, \omega_i) - \mathbf{F}_i(\hat{\mathbf{x}}, \delta_i, \omega_i)$$
$$= \mathbf{F}_i(\mathbf{x}, \delta_i, \omega_i) - \mathbf{F}_i(\hat{\mathbf{x}}, \delta_i, \omega_i) - \Delta\mathbf{F}_i(\mathbf{x}, \delta_i, \omega_i),$$

which, when inserted into (20), gives the following observer error system dynamics:

$$\dot{\tilde{v}}_x = \tilde{v}_y r - \sum_{i=1}^{4} K_i(a_x, \boldsymbol{\omega})\tilde{v}_x + u_1, \tag{25a}$$

$$\dot{\tilde{v}}_y = -\tilde{v}_x r + K_{v_y} \sum_{i=1}^{4} (0\ 1)\mathbf{R}(\delta_i)(\mathbf{F}_i - \hat{\mathbf{F}}_i) + u_2, \tag{25b}$$

$$\dot{\tilde{r}} = \frac{1}{J_z} \sum_{i=1}^{4} \mathbf{g}_i^\mathsf{T} \mathbf{R}(\delta_i)(\mathbf{F}_i - \hat{\mathbf{F}}_i) - K_r \tilde{r} + u_3, \tag{25c}$$

where u_1 is defined in (9), and

$$u_2 = -K_{v_y} \sum_{i=1}^{4} (0\ 1)\mathbf{R}(\delta_i)\Delta\mathbf{F}_i(\mathbf{x}, \delta_i, \omega_i),$$

$$u_3 = -\frac{1}{J_z} \sum_{i=1}^{4} \mathbf{g}_i^\mathsf{T} \mathbf{R}(\delta_i)\Delta\mathbf{F}_i(\mathbf{x}, \delta_i, \omega_i).$$

Let $\mathbf{u} = (u_1, u_2, u_3)^\mathsf{T}$. Theorem 3 shows exponential stability when $\mathbf{u} = 0$. For $\mathbf{u} \neq 0$, a similar procedure as the one leading to

Corollary 2 can be used. Under the assumptions of Theorem 3

$$\dot{V} \leqslant -\lambda_{\min}(A)\|\tilde{\mathbf{x}}\|^2 + \|\tilde{\mathbf{x}}\|\|\mathbf{u}\|,$$

implying that

$$\|\tilde{\mathbf{x}}(t)\| \leqslant \|\tilde{\mathbf{x}}(t_0)\|e^{-\lambda_{\min}(A)/2(t-t_0)} + \frac{2}{\lambda_{\min}(A)}\left(\sup_{t_o \leqslant \tau \leqslant t} \|\mathbf{u}(\tau)\|\right), \tag{26}$$

assuming the supremum exists. We can state the following local ISS result:

Corollary 3. *Assume that the conditions of Theorem 3 hold for all $(\boldsymbol{\delta}, \boldsymbol{\omega}) \in \varDelta \times \varOmega$ on $\|\tilde{\mathbf{x}}\| \leqslant d_x$ and $\|\mathbf{u}\| \leqslant d_u$. Then there exist positive constants k_1 and k_2 such that (26) holds for $\|\tilde{\mathbf{x}}(t_0)\| < k_1$ and $\sup_{t>t_0} \|\mathbf{u}(t)\| < k_2$.*

When $\mathbf{u} = 0$ in (25), the remaining error dynamics depend only on the friction model used in the observer. If one makes sure that this friction model fulfills the following mild conditions:

- Assumption 2 holds globally (one must avoid singularities in slip definitions); and
- the friction model errors $\Delta\mathbf{F}_i$ are bounded (note that the real friction forces are bounded),

then the observer states are globally bounded:

Corollary 4. *Assume that Assumption 2 holds for all $\hat{\mathbf{x}}$ ($X(\boldsymbol{\delta}, \boldsymbol{\omega}) = \mathbb{R}^n$) for the friction model used in the observer, and that the observer gains are chosen according to (21)–(23). Furthermore, assume that $\mathbf{u}$ is bounded. Then the observer error is (uniformly) globally bounded.*

Proof. Since Assumption 2 holds for all $\hat{\mathbf{x}} \in \mathbb{R}^n$, Theorem 3 shows global exponential stability of (25) when $\mathbf{u} = 0$. In the general case, $\mathbf{u} \neq 0$, for which (26) now holds globally. Thus, boundedness of $\mathbf{u}$ implies boundedness of $\tilde{\mathbf{x}}$. $\square$

This result clearly implies that if the real vehicle states are bounded, then under the assumptions of Corollary 4, the observer states are always bounded.

Remark 3. Corollary 4 requires boundedness of u_i. At first sight, it might appear that $u_1 = u$ as defined in (9) becomes unbounded when $\alpha_i = \pm\pi/2$ (it is easy to check that the apparent singularity at $\lambda_{i,x} = -1$ in fact is not a singularity). We have that $\alpha_i \to \pi/2$ only when $V_{i,x} \to 0$, and upon closer inspection, we see that $\lim_{V_{i,x}\to 0} u$ is bounded (actually, the limit as stated is undefined, but the one-sided limits are both defined and bounded). Anyway, this is technicalities; the purpose of the term u is to capture the difference between the real longitudinal velocity and the longitudinal velocities calculated by (7). When $V_{i,x} = 0$ this difference is clearly bounded as long as the measurements ω_i are bounded.

6. Experimental results

In this section, the observers are applied to experimental data from a car. The velocity estimates $\hat{v}_x$ and $\hat{v}_y$ are compared to velocity measurements obtained using an optical correlation-based sensor. The gains of the observers are the same in all experiments. In the longitudinal velocity observer, the gains vary between 0 and 200 (but such that $\sum_{i=0}^{4} K_i(a_x, \omega) > 0$ always), whereas $m K_{v_y} = 0.5$ and $K_r = 20$. The initial condition for $\hat{v}_x$ is taken from one of the undriven wheel speeds, whereas the initial conditions for $\hat{v}_y$ and $\hat{r}$ are set to 0. The friction model used is a proprietary, nonlinear friction model of similar complexity to the magic formula tire model.

We consider two sets of experimental data. The first set comes from driving with a sinusoidal-like steering angle on a flat, dry asphalt road ($\mu_H = 1$ is used in the observer). Fig. 4 shows the steering wheel angle, engine torque and brake flag for this data set. The observer velocities for the modular observer are compared to the measured velocities in Fig. 5. The results for the combined observer are not shown for this data set since they are virtually identical to the modular approach.

The second data set is more challenging: driving in circle on a flat, icy surface ($\mu_H = 0.3$ is used in the observer). The
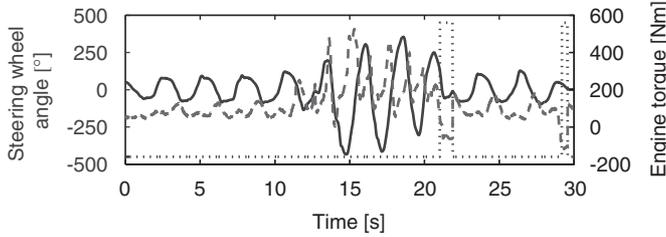

Fig. 4. Steering wheel angle (solid line, left axis) and engine torque (dashed line, right axis) for the first data set. The dotted line shows the binary brake flag.
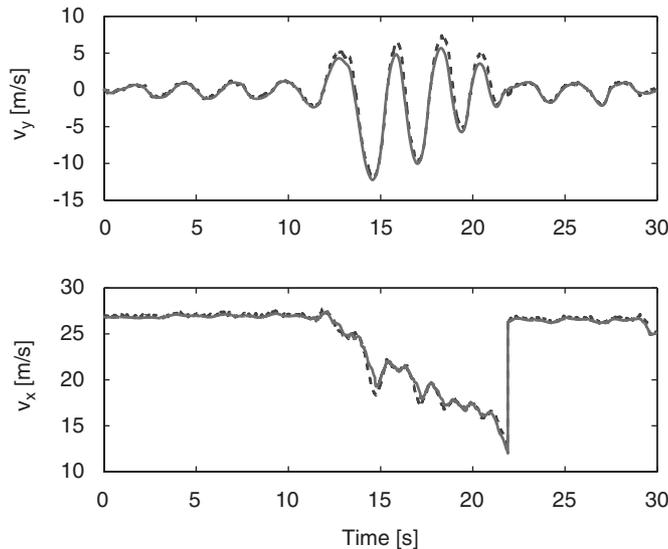

Fig. 5. Estimated (solid) and measured (dashed) lateral velocity (top) and longitudinal velocity (bottom), first data set.
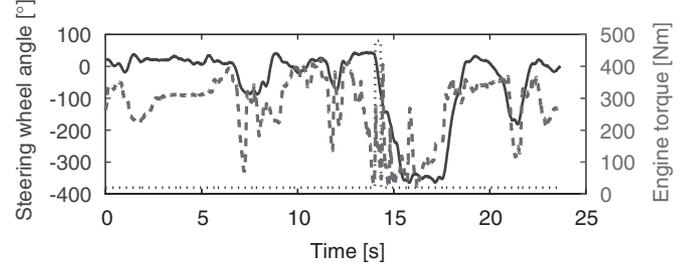

Fig. 6. Steering wheel angle (solid line, left axis) and engine torque (dashed line, right axis) for the second data set. The dotted line shows the binary brake flag.
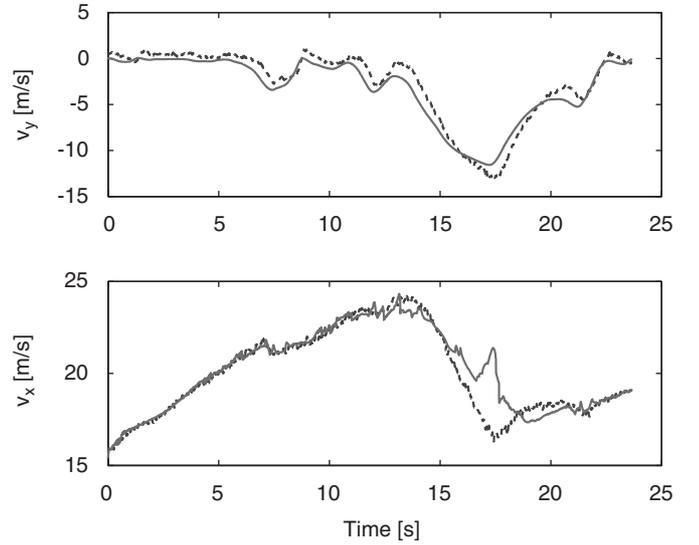

Fig. 7. Estimated (solid) and measured (dashed) lateral velocity (top) and longitudinal velocity (bottom), second data set, modular observer.

steering wheel angle, engine torque and brake flag are shown in Fig. 6. The measured velocities are compared to the velocity estimates from the modular observer in Fig. 7, and with the estimates from the combined observer in Fig. 8.

We make the following observations:

- The results on dry asphalt (Fig. 5) are very good.
- The lateral velocity estimates from the second data set (circle on ice) are also acceptable, although it contains larger errors. The lower accuracy can be attributed mainly to an actual change in road surface conditions, as the vehicle slides off the test track around $t = 15\,\text{s}$, meaning the assumption of constant μ_H is violated. The chosen value of $\mu_H = 0.3$ gives the best average performance on this data set.
- In the second data set, the longitudinal velocity estimate from the modular observer has a large error around 17 s. At this point, the gains $K_i(a_x, \omega)$ are low, and hence the longitudinal velocity observer is similar to an open-loop integrator of longitudinal acceleration. The omitted Coriolis term in the modular approach combined with high lateral velocity and yaw rate, leads to a large error. The error is considerably smaller in the combined observer, which takes the Coriolis term into account.
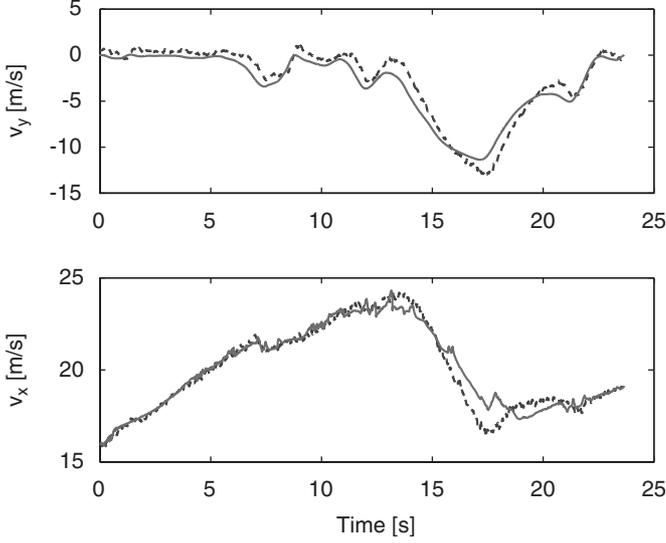
Fig. 8. Estimated (solid) and measured (dashed) lateral velocity (top) and longitudinal velocity (bottom), second data set, combined observer.
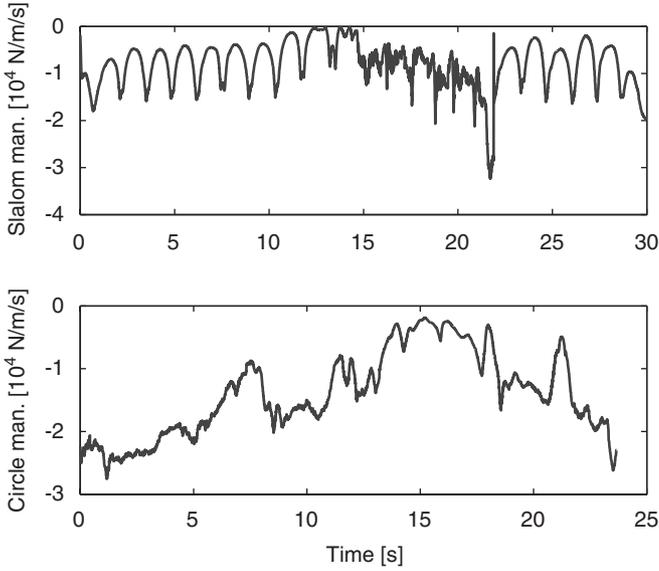

Fig. 9. Condition (3) for first data set (slalom on asphalt, top), and second data set (circle maneuver on ice, bottom).

As a verification of the main convergence assumption (Assumption 2), the condition (3) is calculated based on the friction model, using the velocity estimates and our guess of the maximum friction coefficient. The results are plotted in Fig. 9 for both data sets, and we see that the condition is satisfied in both cases.

7. Discussion

The experiments show that the observers produce good estimates of the lateral velocity, especially on dry asphalt. For the

circle-on-ice data set, the tire-road friction characteristics vary more, resulting in less accurate estimates. The friction model parameter μ_H, the maximum friction coefficient between tire and road, varies with different road conditions. We have assumed that μ_H is constant and known, but in general it must be measured using specially developed sensor systems or adapted based on the available data. Using a too high value for μ_H leads to smaller errors than using one that is too small. An alternative to using a full friction model could be to calculate the lateral friction forces based on measured longitudinal friction forces, similar to van Zanten (2000).

A non-zero road bank angle introduces a gravity component in the lateral acceleration measurement. This can be viewed as a bounded perturbation entering the error dynamics in the same way as u_2 in (25b), and hence an ISS result as in Corollary 3 holds for this input. The road bank angle does not affect the injection term in (19b), as it does not influence the alignment of the friction forces and the acceleration sensor. From this it follows that increasing K_{v_y} reduces the effect of a non-zero road bank angle on the estimate of v_y.

The ISS of the observer error dynamics (Corollaries 1 and 2) implies that a small u (9) results in a small observer error. Whenever the wheel slips are small (normal driving), u is small. When the wheel slips are high, the functions $K_i(a_x, \omega)$ become small such that u is still small. In this case, the longitudinal velocity observer approaches an open loop integrator of the longitudinal acceleration $v_y r + a_x$ (or just a_x in the modular observer). Sensor noise is then integrated and deteriorates the v_x estimate. If the time period with large slips is relatively short, as it typically is, the v_x estimate does not drift much before the wheel speeds can be used to correct the estimate again.

The main advantage of using nonlinear observers compared to an EKF is reduced computational complexity. While the number of ODEs to solve for an EKF is $3/2n + 1/2n^2$, where n is the number of estimated variables, nonlinear observers usually have to solve only n ODEs. Additionally, in an EKF, the nonlinear model must be linearized at each sample, which, along with monitoring of boundedness of the covariance matrix estimate, may involve considerable computation.

The fact that there are few tuning knobs in the observer simplifies tuning compared to tuning the covariance matrix of an EKF. For example, the observer for lateral velocity in the modular approach has only two tuning knobs, with some hints from the theoretical stability conditions as to how the gains may be set.

The effect of measurement errors such as bias in the acceleration and yaw rate measurements are not considered herein, as they can be handled using standard techniques. Attention to such practical issues is nevertheless important for observer performance.

8. Conclusion

Nonlinear observers for vehicle velocity and side-slip have been proposed, and ISS-type stability properties have been proven for these observers under a condition on the friction

model. The observers perform well when applied to experimental data from a car.

Appendix A. Discussion of Assumption 2

This appendix discusses Assumption 2 for two different friction models. Most friction models can be written as a function of lateral and longitudinal tire slips $\mathbf{F}_i = \mathbf{F}_i(\lambda_{i,x}, \lambda_{i,y})$ only,[6] and they therefore depend only indirectly on vehicle velocity. Therefore, we can write the partial derivatives

$$\frac{\partial F_{i,x}}{\partial v_y} = \frac{\partial F_{i,x}}{\partial \lambda_{i,x}}\frac{\partial \lambda_{i,x}}{\partial v_y} + \frac{\partial F_{i,x}}{\partial \lambda_{i,y}}\frac{\partial \lambda_{i,y}}{\partial v_y} = \frac{\partial F_{i,x}}{\partial \lambda_{i,y}}\cos\alpha_i\frac{\partial \alpha_i}{\partial v_y},$$

$$\frac{\partial F_{i,y}}{\partial v_y} = \frac{\partial F_{i,y}}{\partial \lambda_{i,x}}\frac{\partial \lambda_{i,x}}{\partial v_y} + \frac{\partial F_{i,y}}{\partial \lambda_{i,y}}\frac{\partial \lambda_{i,y}}{\partial v_y} = \frac{\partial F_{i,y}}{\partial \lambda_{i,y}}\cos\alpha_i\frac{\partial \alpha_i}{\partial v_y},$$

where we have assumed $\partial \lambda_{i,x}/\partial v_y = 0$. Since

$$\frac{\partial \alpha_i}{\partial v_y} = \frac{-1}{1 + \tan^2(\delta_i - \alpha_i)} < 0,$$

we see that the partial derivatives of the friction model with respect to the lateral slip determine if Assumption 2 holds, assuming $\alpha_i < \pi/2$.

A.1. Linear friction models

In linear friction models it is assumed that the friction forces are proportional to the slips,

$$F_{i,x}(\lambda_{x,i}, \lambda_{y,i}) = C_x\lambda_{i,x},$$

$$F_{i,y}(\lambda_{x,i}, \lambda_{y,i}) = C_y\lambda_{i,y},$$

where C_x and C_y are tire (slip and cornering) stiffness coefficients. Because C_y is generally positive, we conclude that Assumption 2 holds for $\bar{\alpha} < \pi/2$, as pointed out in Remark 1.

A.2. The magic formula tire model

The *magic formula tire model* (Pacejka, 2002) is a widely used semi-empirical model for calculating steady-state tire forces. The *combined slip* magic formula provides formulas for lateral and longitudinal tire forces,

$$F_x(\lambda_x, \lambda_y) = G_x(\lambda_y)F_{x0}(\lambda_x),$$

$$F_y(\lambda_x, \lambda_y) = G_y(\lambda_x)F_{y0}(\lambda_y),$$

where we have simplified somewhat since one of the parameters in G_x (G_y) that according to Pacejka (2002) depends on λ_x (λ_y) is assumed constant. For notational convenience, we drop the dependence on wheel index i in this section. The functions F_{x0} and F_{y0} are the *pure slip* formulas,

$$F_{x0}(\lambda_x) = D_x\sin\zeta_x, \qquad F_{y0}(\lambda_y) = D_y\sin\zeta_y,$$

---

[6] Some friction models may depend on tire slip angles α_i or $\tan\alpha_i$ instead of $\lambda_{i,y} = \sin\alpha_i$, but this does not change the analysis.

where

$$\zeta_x = C_x\arctan\{B_x\lambda_x - E_x(B_x\lambda_x - \arctan B_x\lambda_x)\},$$

$$\zeta_y = C_y\arctan\{B_y\lambda_y - E_y(B_y\lambda_y - \arctan B_y\lambda_y)\}.$$

The functions G_x and G_y are defined as $G_x(\lambda_y) = \cos\eta_x$ and $G_y(\lambda_x) = \cos\eta_y$, where

$$\eta_x = C_{Gx}\arctan\{B_{Gx}\lambda_y - E_{Gx}(B_{Gx}\lambda_y - \arctan B_{Gx}\lambda_y)\},$$

$$\eta_y = C_{Gy}\arctan\{B_{Gy}\lambda_x - E_{Gy}(B_{Gy}\lambda_x - \arctan B_{Gy}\lambda_x)\}.$$

We then have that

$$\frac{\partial F_y}{\partial \lambda_y} = G_y(\lambda_x)\frac{B_yC_yD_y(1 - E_y(1 - 1/(1 + B_y^2\lambda_y^2)))\cos\zeta_y}{1 + \zeta_y^2}.$$

Since $G(\lambda_x) > 0$ and $E_y \leqslant 1$ (Pacejka, 2002, p. 189), $\partial F_y/\partial \lambda_y > 0$ for $\zeta_y < \pi/2$. If the *shape factor* $C_y < 1$, $\partial F_y/\partial \lambda_y > 0$ holds for all λ_y. If $C_y > 1$, the friction force declines for large λ_ys, and $\partial F_y/\partial \lambda_y > 0$ only to the left of the peak of the friction curve, that is, for $|\lambda_y| \leqslant \bar{\lambda}$, where $\bar{\lambda}$ is defined by the solution of

$$E_y = \frac{B_y\bar{\lambda} - \tan\pi/(2C_y)}{B_y\bar{\lambda} - \arctan(B_y\bar{\lambda})}.$$

Furthermore,

$$\frac{\partial F_x}{\partial \lambda_y} = -F_{x0}(\lambda_x)\frac{B_{Gx}C_{Gx}(1 - E_{Gx}(1 - 1/(1 + B_{Gx}^2\lambda_y^2)))\sin\eta_x}{1 + \eta_x^2}.$$

We see that $\text{sign}\,\partial F_x/\partial \lambda_y = -\text{sign}\,(\lambda_x\lambda_y)$, since $\text{sign}\,F_{x0}(\lambda_x) = \text{sign}\,\zeta_x = \text{sign}\,\lambda_x$ and $\text{sign}\,\eta_x = \text{sign}\,\lambda_y$.

From the above, we make the following observations:

- For sufficiently small tire side-slip angles (that is, $|\lambda_y| < \bar{\lambda}$) and small δ, the first part of (3) is negative and dominates the second part.
- For $\lambda_x \approx 0$, the second part of (3) is approximately zero and therefore dominated by the first part.
- For large side-slip angles, the first part of (3) will get less negative, or even positive if $C_y > 1$. However, in the case of braking ($\lambda_x < 0$), the second part of (3) often contributes to fulfilling the assumption: typically $\text{sign}\,\alpha = \text{sign}\,\delta$, and together with $\text{sign}\,\partial F_x/\partial v_y = \text{sign}\,\lambda_x\,\text{sign}\,\alpha$ this gives $(\partial F_x/\partial v_y)\sin\delta < 0$.

We conclude that (3) is negative for realistic slip values and sufficiently small steering angles, for tires with $C_y < 1$. For tires with $C_y > 1$, (3) may be positive for some combinations of λ_x and large λ_y. Because (3) is a sum over all wheels, it is possible for the entire expression to be negative despite positive contributions from some wheels. For instance, rear wheels will often have lower tire side-slip angles due to small steering angle values.

When a friction model with computable partial derivatives is available, (3) can be evaluated based on the estimates. Since (3) essentially is the only assumption that is required for the

analysis herein, one might consider using the computed value for convergence monitoring, somewhat akin to monitoring covariances in an EKF, and to take corrective steps if it becomes positive.

The above discussion shows that the only situations in which Assumption 2 might not hold are situations with large lateral slip values. From physical considerations, we know that such situations can only be sustained for limited time intervals. As shown in Corollary 4, if the friction model used in the observer fulfills Assumption 2, the observer states always remain bounded, including during these time intervals. It is therefore not crucial if Assumption 2 should not hold for the real friction forces for all possible slip values.

The experimental validation in Section 6 (Fig. 9) indicate that for the friction model used in the observer (which was not modified in any way for use in the observer), Assumption 2 is fulfilled at all times.

References

Angeli, D., & Sontag, E. D. (1999). Forward completeness, unboundedness observability, and their Lyapunov characterizations. *Systems Control Letters*, *38*(4–5), 209–217.

Best, M. C., Gordon, T. J., & Dixon, P. J. (2000). An extended adaptive Kalman filter for real-time state estimation of vehicle handling dynamics. *Vehicle System Dynamics*, *34*, 57–75.

Farrelly, J., & Wellstead, P. (1996). Estimation of vehicle lateral velocity. *Proceedings of the 1996 IEEE international conference on control applications* (pp. 552–557).

Fukada, Y. (1999). Slip-angle estimation for stability control. *Vehicle Systems Dynamics*, *32*, 375–388.

Hac, A., & Simpson, M. D. (2000). Estimation of vehicle side slip angle and yaw rate. In *SAE 2000 World Congress*. Detroit, MI, USA.

Hiemer, M., vonVietinghoff, A., Kiencke, U., & Matsunaga, T. (2005). Determination of vehicle body slip angle with non-linear observer strategies. In *Proceedings of the SAE World Congress*. Paper no. 2005-01-0400.

Imsland, L., Johansen, T. A., Fossen, T. I., Kalkkuhl, J., & Suissa, A. (2005). Vehicle velocity estimation using modular nonlinear observers. In *Proceedings of 44th IEEE Conference Decision Control*.

Kalkkuhl, J., Johansen, T. A., & Ludemann, J. (2003). Nonlinear adaptive backstepping with estimator resetting using multiple observers. In: R. Johansson, & A. Rantzer (Eds.), *Nonlinear and hybrid systems in automotive control* Berlin: Springer.

Khalil, H. K. (2002). *Nonlinear systems*. 3rd ed., Upper Saddle River, NJ: Prentice-Hall.

Kiencke, U., & Daiss, A. (1997). Observation of lateral vehicle dynamics. *Control Engineering Practice*, *5*(8), 1145–1150.

Kiencke, U., & Nielsen, L. (2000). *Automotive control systems*. Berlin: Springer.

Lu, J., & Brown, T. A. (2003). *Vehicle side slip angle estimation using dynamic blending and considering vehicle attitude information*. Patent US 6671595.

Pacejka, H. B. (2002). *Tyre and vehicle dynamics*. London: Butterworth-Heinemann.

Ray, L. R. (1995). Nonlinear state and tire force estimation for advanced vehicle control. *IEEE Transactions on Control Systems Technology*, *3*(1), 117–124.

Ray, L. R. (1997). Nonlinear tire force estimation and road friction identification: Simulation and experiments. *Automatica*, *33*(10), 1819–1833.

Sontag, E. D., & Wang, Y. (1995). On characterizations of the input-to-state stability property. *Systems Control Letters*, *24*(5), 351–359.

Suissa, A., Zomotor, Z., & Böttiger, F. (1996). *Method for determining variables characterizing vehicle handling*. Patent US 5557520.

Ungoren, A. Y., Peng, H., & Tseng, H. (2004). A study on lateral speed estimation methods. *International Journal on Vehicle Autonomous Systems*, *2*(1/2), 126–144.

van Zanten, A.T. (2000). Bosch ESP system: 5 years of experience. In *Proceedings of the automotive dynamics & stability conference* (p. 354). Paper no. 2000-01-1633.

Venhovens, P. J. T., & Naab, K. (1999). Vehicle dynamics estimation using Kalman filters. *Vehicle System Dynamics*, *32*, 171–184.